Digital Compensation of Sampling Frequency Offset for OFDM-based Visible Light Communication Systems

Qingqing Hu[1], Xianqing Jin[1], Zhengyuan Xu[1,2]
[1]Key Laboratory of Wireless-Optical Communications, Chinese Academy of Sciences,
University of Science and Technology of China, Hefei, Anhui 230026, China
[2]Shenzhen Graduate School, Tsinghua University, Shenzhen 518055, China
E-mail: {xqjin, xuzy}@ustc.edu.cn

Abstract— **Sampling frequency offset (SFO), which is due to mismatch of sampling clocks between transmitter and receiver oscillators, is a key factor affecting transmission performance of orthogonal frequency division multiplexing (OFDM) signal in visible light communication (VLC) systems with bandwidth-limited light emitting diodes (LEDs). To improve the system spectral efficiency for a relatively high capacity, an effective scheme for SFO compensation is required to achieve a high signal to interference plus noise ratio (SINR). From the practical system design point of view, a fourth-order piecewise polynomial interpolator using Farrow structure is proposed to digitally compensate SFO for VLC systems. Nonlinearity of LEDs causes extra high frequency components beyond the OFDM signal spectrum, which may aggravate the aliasing effect when digital compensation of SFO is applied. Theoretical study is thus given to the impact of both the LED nonlinearity and SFO-induced inter-carrier interference (ICI) on SINR of the received OFDM signal. Both numerical and experimental results show that the proposed scheme can be applied to effectively compensate a local oscillator frequency offset up to ±1000ppm in an OFDM-based VLC system at a minimum oversampling rate of 1.3 at the receiver.**

Keywords— Visible light communication (VLC); orthogonal frequency division multiplexing (OFDM); sampling frequency offset (SFO); synchronization

I. INTRODUCTION

To address the challenge of limited bandwidth in the current wireless communication systems, visible light communication (VLC) has been considered as a promising technology for future high-speed and/or green communication systems due to the rich license-free spectrum (380-780nm) of widely deployed light emitting diodes (LEDs) as energy-efficient light source for both illumination and communication [1-3]. In theory, VLC can offer a 1000 times greater bandwidth compared to the radio frequency (RF) communications. Since LEDs have a feature of fast-switching for amplitude modulation, intensity modulation/direct detection (IMDD) is applied in a cost-effective VLC system with commercially available white LEDs, which results in limited modulation bandwidth of several MHz without optical filtering and equalization. In order to improve signal spectral efficiency for high-speed VLC transmission [3, 4], orthogonal frequency division multiplexing (OFDM) has been widely investigated in recent years. In an OFDM-based VLC system with high spectral efficiency, a relatively precise synchronization is required since sampling frequency offset (SFO) occurs due to mismatch of sampling clocks between transmitter and receiver oscillators, which results in severe interference between adjacent OFDM subcarriers (inter-carrier interference, ICI) [5, 6]. In practice, the inherent instability of transmitter and receiver oscillators causes clock frequency to fluctuate with time and temperature. Many standards for wireless communication systems specify an acceptable packet error rate for clocks with a tolerance of ±20~25ppm [7]. In addition, there are nonlinear regions in the *P-U* curve of LEDs due to saturation of output optical power. Such nonlinearity causes extra new frequency components inside/outside the OFDM signal spectrum, which may affect the synchronization performance.

There are several different methods for the sampling frequency synchronization, which can be categorized in the following two types: 1) *Synchronous mode*: Sampling at the receiver can be synchronized to the symbol rate of the incoming signal with feedback/feedforward information about estimated SFO for adjustment of the phase of a local clock [8-11]. Such a method has a large timing fluctuation due to high-level phase noise [12]. The receiver clock can also be synchronized by sending a dedicated clock signal along with information signal, which can be extracted at the receiver [13, 14]. However, this method requiring additional analog circuits increases not only system complexity, but also peak-to-average power ratio (PAPR) of OFDM signal. 2) *Asynchronous mode*: Digital processing of sampled signal is applied to mitigate SFO effect without altering the local clock. This can be realized by multiplying the signal after fast Fourier transform (FFT) (or before inverse FFT) with an exponential term derived from the estimated SFO to compensate phase error at each subcarrier at the receiver (or transmitter) [15-23], or interpolating the sampled signal to construct a resampled signal at the same sampling frequency as the transmitter [24]. For the former scheme of digital SFO compensation using the phase rotation correction term, SFO effect can be partially mitigated because the ICI between subcarriers due to the SFO still exists. For the latter scheme using digital interpolation, the ICI can be well alleviated in the digitally resampled signal so that the SFO effect is expected to be mitigated completely.

978-1-5386-4328-0/18/$31.00 ©2018 IEEE

In the previously published work, there is rare study about digital compensation of SFO with interpolation for OFDM-based VLC applications. In this paper, investigation is made of exploring an efficient scheme for digital compensation of SFO in the high-speed OFDM-based VLC system. To understand the combined nonlinear and aliasing effect during digital processing of SFO compensation at the receiver, the impact of both the LED nonlinearity and SFO-induced ICI on signal to interference plus noise ratio (SINR) is theoretically investigated in an OFDM-based VLC system. With a fundamental model of the nonlinear LED-based VLC channel, a fourth-order piecewise polynomial interpolator using Farrow structure is proposed to digitally compensate SFO estimated with scattered pilots. In addition, it is desirable to use an analog-digital converter (ADC) operating at a low sampling frequency at the receiver for low complexity. Special attention is given to numerical and experimental exploration of the minimum oversampling rate of the ADC required for achieving the improved transmission with the proposed scheme.

II. Digital compensation of SFO with polynomial interpolator using Farrow structure

Figure 1 shows a block diagram of a typical OFDM-based VLC system with an LED. At the transmitter, real-valued OFDM signal generated with input data of IFFT satisfying Hermitian symmetry is sent to a digital-analog converter (DAC) at a sampling frequency of f_t. The analog OFDM signal is then used to directly drive the LED for VLC transmission. At the receiver, optical intensity of the received OFDM signal is detected with a photodiode (PD). The electrical OFDM signal is digitized with an ADC at a sampling frequency of f_s before signal recovery in digital signal processing including synchronization, FFT and equalization. Given the instability of transmitter/receiver oscillators, the frequency of receiver clock is defined as $f_s = 1/T_s = \lambda f_t(1+\eta)$, where λ is oversampling rate and η is SFO. The SFO is estimated and digitally compensated as shown in Fig. 2. In this section, theoretical investigation is given to the proposed digital compensation of SFO with a polynomial interpolator using Farrow structure. The SINR due to the SFO-induced ICI and LED nonlinearity is also analytically studied.

A. Sampling frequency offset (SFO)

For simplicity of analysis of the SFO effect, a linear channel is initially assumed. The demodulated OFDM signal at the k^{th} subcarrier of the l^{th} OFDM symbol after FFT in Fig. 1 is written as [5]:

$$Y_l(k) = e^{j\pi\phi_{k,k}(N-1)/N} \cdot e^{j2\pi\phi_{k,k}(lN_s+N_g)/N} \cdot \frac{\sin(\pi\phi_{k,k}) \cdot Z_l(k)H_l(k)}{N\sin(\pi\phi_{k,k}/N)} + \sum_{i=0,i\neq k}^{N-1} e^{j\pi\phi_{i,k}(N-1)/N} \cdot e^{j2\pi\phi_{i,k}(lN_s+N_g)/N} \cdot \frac{\sin(\pi\phi_{i,k}) \cdot Z_l(i)H_l(i)}{N\sin(\pi\phi_{i,k}/N)} + n_l(k) \quad (1)$$

$$\phi_{i,k} = (1+\eta)i - k \quad (2)$$

where N and N_g are size of inverse FFT (IFFT) and cyclic prefix, respectively. The symbol length N_s is thereby equal to (N+N_g). Z_l and H_l are transmitted OFDM signal and frequency response of the VLC channel, respectively. n_l is complex noise. As seen from (1), the SFO causes amplitude attenuation, phase rotation and ICI. Before the digital SFO compensation, the SFO is estimated with scattered pilots after FFT in the frequency domain [23]. The phase rotation of the k^{th} pilot subcarrier in the l^{th} OFDM symbol is given by $\varphi_{l,k} = \pi\phi_{k,k}(N-1)/N + 2\pi\phi_{k,k}(lN_s+N_g)/N$. With the phase difference of pilots between two OFDM symbols delayed by D symbols (pilot period), $\vec{\theta}_{l,k} = \vec{\varphi}_{l,k} - \vec{\varphi}_{l-D,k} = 2\pi N_s D\eta\vec{k}/N$, the estimated SFO, $\hat{\eta}$, is obtained with (L-D) symbols

$$\hat{\eta} = \hat{A}N/(2\pi N_s D) \quad (3)$$

$$\hat{A} = \sum_{l=D+1}^{L}\sum_{i=1}^{p} k_i\theta_{l,k_i} \Big/ (L-D)\sum_{i=1}^{p} k_i^2 \quad (4)$$

where k_i is pilot index. In Fig. 2, a feedback loop is applied to track SFO at a resampling frequency given below

$$f_i = 1/T_i = f_i'/(1+\hat{\eta}) \quad (5)$$

where f_i' is the calculated resampling frequency in the previous loop and its initial value is f_s/λ.

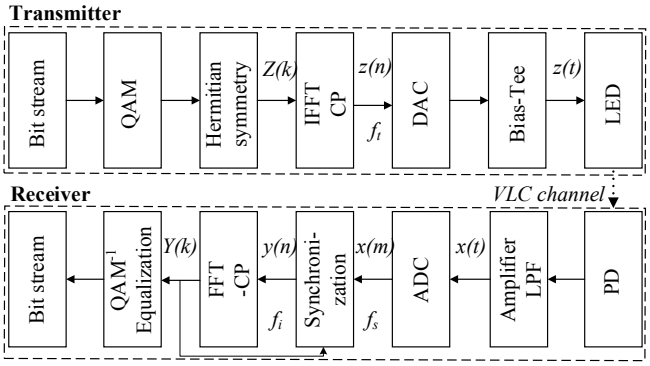

Fig. 1. A typical OFDM-based VLC system with an LED.

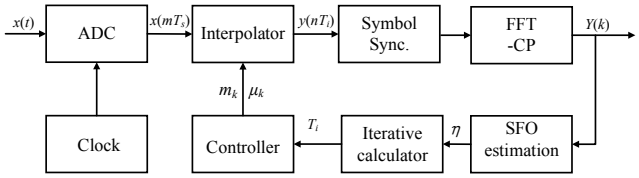

Fig. 2. Digitial compensation of SFO with polynomial interpolator.

B. Digital compensation of SFO

With the estimated SFO, a piecewise polynomial interpolator with Farrow structure is used to construct resampled signal for SFO compensation. The advantage of the polynomial interpolator is that the interpolation signal can be calculated without storing samples for calculation of impulse response. The resampled signal $y(nT_i)$ is written as [24, 25]

$$y(nT_i) = \sum_m x(mT_s)h_I(nT_i - mT_s) \quad (6)$$

where h_I is impulse response of the digital interpolator. With the polynomial interpolation using Farrow structure for high-

speed systems, (6) can be derived in the following form [24, 25],

$$y(nT_i) = y((m_k + \mu_k)T_s) = \sum_{i=I_1}^{I_2} x[(m_k - i)T_s]h_I[(i + \mu_k)T_s] \quad (7)$$

$$m_k = \text{int}\left[nT_i / T_s\right], \quad \mu_k = nT_i / T_s - m_k, \quad i = m_k - m \quad (8)$$

$$h_I[(i + \mu_k)T_s] = \sum_{q=0}^{Q} c_q(i)\mu_k^q \quad (9)$$

where $c_q(i)$ is coefficient of the interpolation filter. Here, a fourth-order piecewise polynomial interpolator ($Q=4$) using Farrow structure is proposed to improve the VLC transmission performance by suppressing the spectral artifacts more than 60dB below the designed passband [26]. To verify the improved transmission performance, the piecewise-parabolic *(Q=2)* and cubic *(Q=3)* interpolation filters are also investigated. Figure 3(a) shows spectrum difference between the 2nd (piecewise-parabolic), 3rd (cubic) and 4th order interpolation filters. The amplitude of the spectrum for the 4th order case is less attenuated than the 2nd and 3rd order cases when $fT_s < 0.5$, but attenuates faster when $fT_s \geq 0.5$.

The controller is designed to calculate integer index m_k and fractional interval μ_k for the input of interpolator with the calculated T_i from the iterative calculator

$$m_{k+1} = m_k + \text{int}\left[\mu_k + T_i / T_s\right] \quad (10)$$

$$\mu_{k+1} = (\mu_k + T_i / T_s) - \text{int}[\mu_k + T_i / T_s] \quad (11)$$

where int[μ] means the largest integer not exceeding μ.

C. SINR due to SFO-induced ICI and LED nonlinearity

To focus on theoretical investigation of performance of SFO compensation, the DAC is assumed to be ideal. At the transmitter, the LED is driven by an electrical OFDM signal $z(t)$, which can be expressed as

$$z(t) = V_b + \frac{u}{2}\left[\sum_{k=1}^{N/2-1} Z(k)e^{j2\pi k\Delta ft} + \sum_{k=1}^{N/2-1} Z^*(k)e^{-j2\pi k\Delta ft}\right] \quad (12)$$

where V_b is bias voltage, u is an electrical gain factor, Δf is subcarrier spacing. Cyclic prefix is ignored to simplify the analysis here.

To model the LED nonlinearity, a second-order polynomial form is used to mimic the measured *P-U* curve of the LED as shown in Fig. 3(b), whilst Fig. 3(c) shows frequency response of the LED. The optical power of the signal from the LED is given by [27]

$$p(t) = b_2 z^2(t) + b_1 z(t) + b_0 \ . \quad (13)$$

where b_i is coefficient of the polynomial function. In the frequency domain, (13) can be written as

$$P(k \cdot \Delta f) = \begin{cases} MZ(k) + C(k), & k \in (0, N/2 - 1] \\ \dfrac{u^2 b_2}{4}\sum_{G_k} Z(m)Z(l), & k \in [N/2, N-1) \end{cases} \quad (14)$$

$$M = \frac{u(b_1 + 2b_2 V_b)}{2} \quad (15)$$

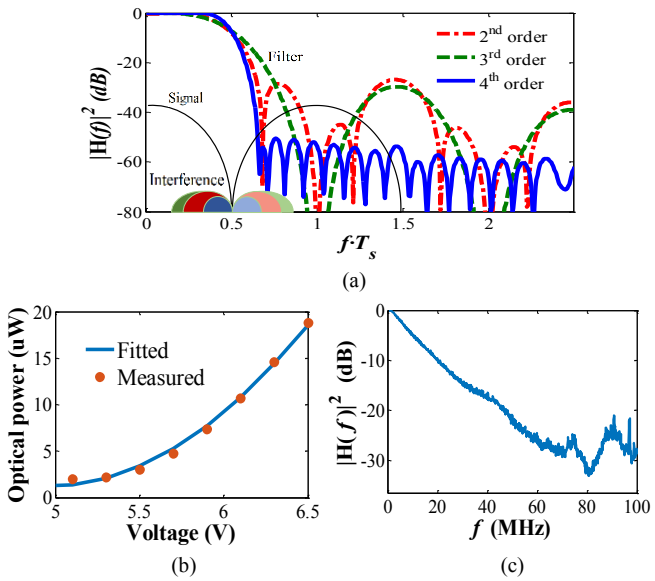

Fig. 3. (a) Spectra of interpolation filters using Farrow structure and the aliasing effect, (b) P-U curves, Markers/Solid curve: measured/fitted curve, (c) Frequency response of the LED.

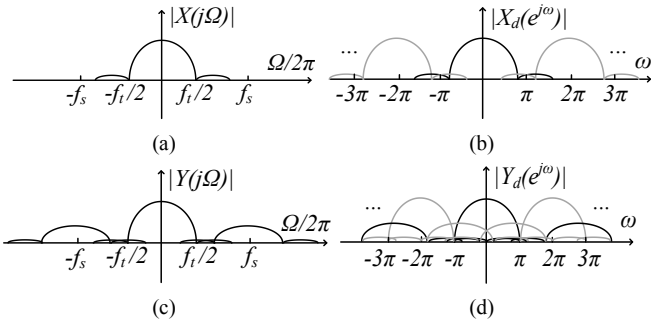

Fig. 4. Spectra of signals (a) $x(t)$, (b) $x(m)$, (c) $y(t)$, (d) $y(n)$. $\Omega = 2\pi f = \omega/T$.

$$C(k) = \frac{u^2 b_2}{4}\left[\sum_{\mathrm{T}_k} Z(m)Z(l) + 2\sum_{\Lambda_k} Z(m)Z^*(l)\right] \quad (16)$$

$$\begin{aligned} \mathrm{T}_k &= \{m,\ l \mid 1 \leq m,\ l \leq N/2 - 1 \ \ \&\ (m + l) = k\} \\ \Lambda_k &= \{m,\ l \mid 1 \leq m,\ l \leq N/2 - 1 \ \ \&\ (m - l) = k\} \\ G_k &= \{m,\ l \mid 1 \leq m,\ l \leq N/2 - 1 \ \ \&\ (m + l) = k\} \end{aligned} \quad . \quad (17)$$

At the receiver, the spectrum of the continuous signal $x(t)$ in Fig. 4(a) can be written as

$$X(j\Omega) = P(j\Omega)H_c(j\Omega) + n(j\Omega) \quad (18)$$

where $\Omega = 2\pi f$. H_c is frequency response of the VLC link including the LED, PD, electrical amplifier and LPF. $P(j\Omega)$ is spectrum of the optical signal after the LED, which can be easily derived from (13). $n(j\Omega)$ is sum of shot noise and thermal noise at the receiver. For simplicity, $n(j\Omega)$ is modeled as additive white Gaussian noise (AWGN) with a variance of σ_n^2 [28]. The LPF is used to partially suppress interferences outside the signal spectrum. The spectrum of $x(m)$ after ADC in Fig. 4(b) is expressed as

$$X_d(e^{j\omega}) = f_s \sum_{r=-\infty}^{\infty} X(j\omega f_s + j2\pi r f_s) \quad (19)$$

where r is an integer number, and $\omega=\Omega/f_s$. The oversampling rate λ of 1~2 at the receiver ADC ($f_s \in [f_t, 2f_t]$) is considered here. As the first sidelobe of the signal spectrum $X(j\Omega)$ contains most power of out-of-band signal, the spectrum of the continuous-time signal reconstructed with interpolation in Figs. 4(c) is calculated as follows

$$Y(j\Omega) = H_I(j\Omega)\sum_{r=-1}^{1} X(j\Omega + j2\pi r f_s) \tag{20}$$

where $H_I(j\Omega)$ is spectrum of the interpolation filter. In Fig. 4(d), the spectrum of the resampled signal $y(n)$ can be derived as

$$Y_d(e^{j\omega}) = f_i \sum_{r_2=-\infty}^{\infty} H_I(j\omega f_i + j2\pi r_2 f_i)\cdot \sum_{r_1=-1}^{1} X(j\omega f_i + j2\pi r_2 f_i + j2\pi r_1 f_s) \tag{21}$$

If SFO is accurately estimated, $f_i \approx f_t$ is satisfied. The signal after FFT can be written as

$$Y(k) = f_i[H(k)Z(k) + I(k) + n_F(k)] \tag{22}$$

$$H(k) = MH_c(k)H_I(k) \tag{23}$$

$$\begin{aligned} I(k) = \sum_{i=1}^{2} & [P(k+(\psi-i)N)H_c(k+(\psi-i)N)H_I(k-iN) \\ & + P(k-(\psi-i)N)H_c(k-(\psi-i)N)H_I(k+iN)] \\ & + C(k)H_c(k)H_I(k) \end{aligned} \tag{24}$$

$$\begin{aligned} n_F(k) = \sum_{i=1}^{2} & [n(k+(\psi-i)N)H_I(k-iN) \\ & + n(k-(\psi-i)N)H_I(k+iN)] + n(k)H_I(k) \end{aligned} \tag{25}$$

where $\psi = \lambda(1+\eta)$. Therefore, the SINR at the k^{th} subcarrier is obtained as

$$SINR_k = \frac{|H(k)|^2 E(|Z(k)|^2)}{E(|I(k)|^2) + E(|n_F(k)|^2)}. \tag{26}$$

As shown in (22)-(26), SINR depends on SFO, oversampling rate at the receiver, and frequency responses of the polynomial interpolator and VLC channel and LED nonlinearity, which are discussed in Section III.

III. Results and Discussion

A. Numerical verification of the digital SFO compensation

Based on the theoretical study of the SFO in the OFDM-based VLC system in Section II, 16-QAM-OFDM transmission performance over the VLC links with an LED is numerically investigated for verification of the proposed digital compensation of SFO with the polynomial interpolator using Farrow structure. The sizes of IFFT and CP are 128, 16, respectively. Pilots at the 12th, 23rd, 34th, and 45th subcarriers are used to estimate SFO. The sampling frequency of DAC is fixed at 25MHz, whilst the bandwidth of OFDM signal is 12.5MHz.

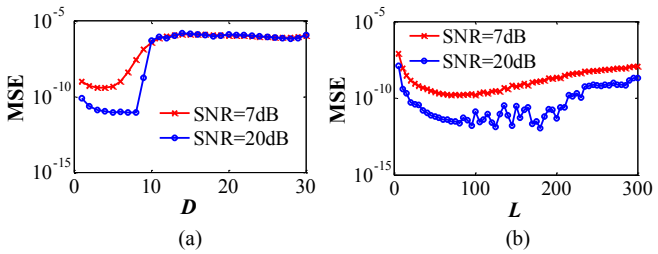

Fig. 5. MSE of SFO as a function of (a) D (L = 40) or (b) L (D = 4) in AWGN, SFO=1000ppm.

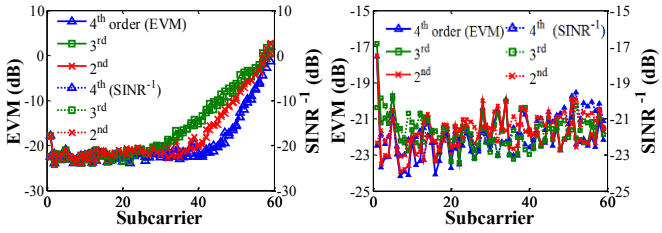

Fig. 6. EVM and SINR performance in an LED-based VLC channel at an oversampling rate of (a) λ =1, (b) λ =1.5. SFO=100ppm.

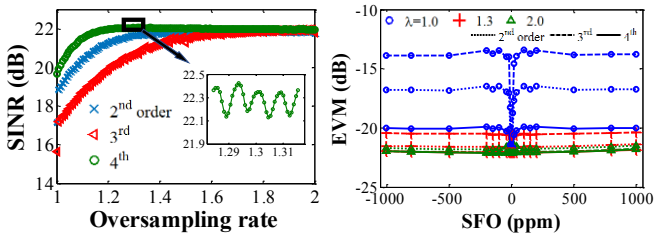

Fig. 7. (a) SINR as a function of oversampling rate. (b) EVM versus SFO with the 2nd, 3rd and 4th order interpolators in an LED-based VLC link.

Before investigation of the OFDM transmission performance, key parameters of D (pilot period) and L (number of symbols for SFO estimation) from (4) are optimized under AWGN in Fig. 5, where *SFO=1000*ppm. Mean square error (MSE) of the estimated SFO is used to quantify the estimation performance. As seen in Fig. 5, the increment of MSE with increasing L or D for SNR=7 or 20dB when $L \geq 40$ or $D \geq 4$ is observed because the estimated phase difference between two pilot symbols must be in the range $[-\pi, \pi]$, and the shift of FFT window due to the SFO must be in the cyclic prefix range. For L *(D)* less than the optimum value of 40 (4), the MSE performance degrades with decreasing L *(D)* because of the noise effect.

With the optimized parameters, L=40 and D=4, error vector magnitude (EVM) and SINR performance over a VLC link with the LED in Figs. 3(b, c) are used to validate the performance of SFO compensation with the 2nd, 3rd and 4th order polynomial interpolators using Farrow structure in Fig. 6, where SFO=100ppm, SNR=28dB. The EVM performance is consistent with the SINR derived from (26). As seen in the figures, the 4th order polynomial interpolator outperforms the 2nd and 3rd order polynomial interpolators at an oversampling rate of 1 or 1.5. Figure 6(a) shows a significantly degraded EVM in the high frequency subcarriers for both cases because

the imperfect interpolation filter and LED-nonlinearity cause out-of-band signal, which interferes the signal on the high-frequency subcarriers during the resampling process as shown in Fig. 3(a). For λ=1.5, the interference on the high-frequency subcarriers disappears in Fig. 6(b). It is noted that the calculated EVM/SINR is worse than the defined SNR of 28dB under the condition of Gaussian noise only because of the LED-nonlinearity induced ICI inside the OFDM spectrum.

Figure 7(a) shows the impact of oversampling rate on the SINR performance under the same condition as Fig. 6. The SINR is improved with increasing oversampling rate until saturation of SINR. The minimum required oversampling rate for the best SINR performance using the 4th order interpolation is approximately equal to 1.3, which is smaller than the 2nd or 3rd order interpolation. Due to orthogonality between adjacent OFDM subcarriers, there is a fluctuation in SINR at around 22dB as seen in the inset. To investigate the impact of SFO on the EVM performance using the proposed scheme for the digital SFO compensation, Fig. 7(b) shows EVM performance as a function of SFO at different oversampling rates from 1.0 to 2.0 in the LED-based VLC channel. It is noted that for |SFO| $\leqslant$1000ppm the EVM for λ=1.3 or 2 reaches minimum, whilst the 4th order interpolation always performs best, which agrees very well with the results in Fig. 6.

B. *Experimental results*

After the numerical verification of the proposed scheme for digital SFO compensation, experimental investigation of the EVM performance of 16-QAM-OFDM signal is conducted over a 6-m VLC link with an LED, which has a 3-dB bandwidth of approximately 6MHz. The experimental setup of the VLC system with the LED and the avalanche photodiode (APD) receiver is depicted in Fig. 8. Independent clocks are applied to introduce SFO between the arbitrary waveform generator (AWG) and digital storage oscilloscope (DSO). Because of discrete values of sampling clocks for the AWG or DSO, parameters of OFDM signal and sampling frequency for the DSO listed in Table I are adopted.

At the transmitter, a 5×10^5 bit pseudo random binary sequence is generated for 16-QAM mapping. Every 40 OFDM symbols form a data block for the SFO estimation. The OFDM signal generated with Matlab is loaded into the AWG (Tektronix 5014C, 14-bit DAC) for an electrical OFDM signal used to drive the LED with a Bias-Tee. The Bias voltage is 5.75V, and the peak-to-peak voltage of driving signal is 0.4V. At the receiver, a lens with a diameter of 10cm is placed in front of APD to collect light for a high optical gain. The light passing through a blue filter is then detected by an APD. After the LPF, the received signal is sampled by a digital storage oscilloscope (DSO, Agilent MSO-X 6004A, 12-bit ADC) for offline signal recovery. The output of the 10MHz reference clock of the AWG is connected to the input of DSO in order to introduce a precise SFO, which is varied by adjusting sampling frequency of the AWG.

As seen in Fig. 9, the constellations of the received 16-QAM-OFDM signal for relatively large SFO before the SFO compensation are rotated and dispersed due to the ICI. The constellation after the SFO compensation is well converged,

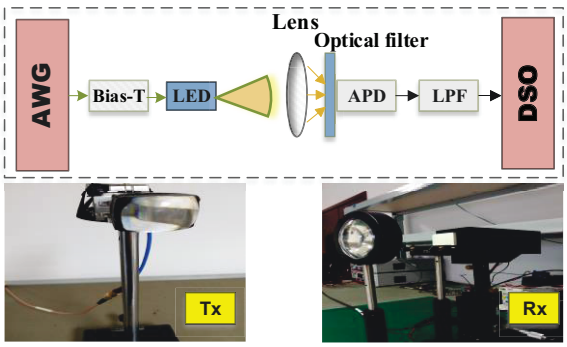

Fig. 8. Experimental setup of the VLC system.

TABLE I. PARAMETERS OF DSO AND OFDM SIGNAL

Oversampling rate, λ	1.0	1.3	1.5	1.7	2.0
f_s of DSO (MHz)	25	25	25	25	50
Signal bandwidth (MHz)	12.5	9.6	8.3	7.4	12.5
Bit rate (Mb/s)	43.8	33.7	29.2	25.7	43.8

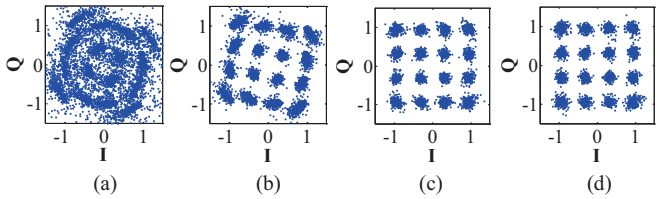

Fig. 9. Constellations of the received 16-QAM-OFDM signal (a)-(c) before or (d) after the SFO compensation. (a)-(c) *SFO*=80, 40, 0ppm, (d) *SFO*=80ppm.

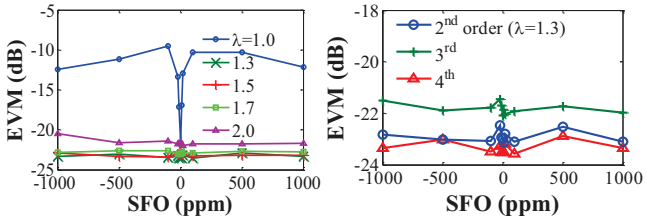

Fig. 10. (a) Measured EVM versus *SFO* at different oversampling rates using the 4th order interpolator. (b) EVM performance with the 2nd, 3rd and 4th order interpolators when λ=1.3.

which is similar to that for SFO = 0. This indicates a valid SFO compensation with the propose scheme.

Figure 10(a) shows the measured EVM performance with the digital SFO compensation at different oversampling rates. The best EVM performance at around -22dB is achieved at an oversampling rate of $\geq$1.3, which is consistent with the numerical results in Fig. 7. The slight variation in EVM for $\lambda\geq$1.3 is due to different bandwidth of the OFDM signals in the experiment. Because the signal with relatively small bandwidth attenuates less than that with relatively large bandwidth, the EVM at λ =1.3, 1.5 or 1.7 is better than that at λ =1.0 or 2.0 when SFO = 0ppm. For EVM comparison between the 2nd, 3rd and 4th order polynomial interpolators, it is seen from Fig. 10(b) that the EVM with the 4th order interpolator is improved by ~0.4dB (1.8dB) as compared with that with 2nd (3rd) order

interpolator. The experimental results, which agree very well with the numerical results, confirm again that the proposed scheme for the digital SFO compensation using the 4th order interpolator can be used to effectively compensate a local oscillator frequency offset up to ±1000ppm in an OFDM-based VLC system with a minimum oversampling rate of 1.3 at the receiver.

IV. CONCLUSIONS

With analytical study of the combined nonlinear and aliasing effect during the digital process of SFO compensation in an OFDM-based VLC system with practical LEDs, a fourth-order piecewise polynomial interpolator using Farrow structure has been proposed to digitally compensate SFO between transmitter and receiver oscillators. Theoretical investigation has been conducted on the impact of both the LED nonlinearity and SFO-induced ICI on SINR of the received OFDM signal. With the optimized parameters for SFO estimation, numerical and experiment results have shown that the proposed interpolator for the digital SFO compensation can be used to effectively compensate a local oscillator frequency offset up to ±1000ppm at a minimum oversampling rate of 1.3 in an OFDM-based VLC system.

ACKNOWLEDGMENT

This work was supported by the National Key Research and Development Program of China (Grant No. 2017YFB0403604), Key Program of National Natural Science Foundation of China (Grant No. 61631018), Key Research Program of Frontier Sciences of CAS (Grant No. QYZDY-SSW-JSC003), and Fundamental Research Funds for the Central Universities (Grant No. WK2100060022).

REFERENCES

[1] A.C. Boucouvalas, P. Chatzimisios, Z. Ghassemlooy, M. Uysal, and K. Yiannopoulos, "Standards for indoor optical wireless communications," IEEE Communications Magazine, vol. 53, no. 3, pp. 24-31, Mar. 2015.

[2] A.V. N. Jalajakumari, E. Xie, J. McKendry, E. Gu, M.D. Dawson, H. Haas, and R. K. Henderson, "High-speed integrated digital to light converter for short range visible light communication," IEEE Photonics Technology Letters, vol. 29, no. 1, pp. 118-121, Jan. 2017.

[3] A.H. Azhar, T. A. Tran, and D. O'Brien, "A Gigabit/s indoor wireless transmission using MIMO-OFDM visible-light communications," IEEE Photonics Technology Letters, vol. 25, no. 2, pp. 171-174, Jan. 2013.

[4] H. Elgala, R. Mesleh, and H. Haas, "Indoor broadcasting via white LEDs and OFDM," IEEE Transactions on Consumer Electronics, vol. 55, no. 3, pp. 1127-1134, Aug. 2009.

[5] M. Speth, S.A. Fechtel, G. Fock, and H. Meyr, "Optimum receiver design for wireless broad-band systems using OFDM. I," IEEE Transactions on Communications, vol. 47, no. 11, pp. 1668-1677, Nov. 1999.

[6] X. Wang, T.T. Tjhung, Y. Wu, and B. Caron, "SER performance evaluation and optimization of OFDM system with residual frequency and timing offsets from imperfect synchronization," IEEE Transactions on Broadcasting, vol. 49, no. 2, pp. 170-177, Jun. 2003.

[7] IEEE, "Telecommunications and information exchange between systems-part 11", High Speed Physical layer in the 5GHz Band, Dec. 1999.

[8] M. Chen, J. He, Z. Cao, J. Tang, L. Chen, and X. Wu, "Symbol synchronization and sampling frequency synchronization techniques in real-time DDO-OFDM systems," Optics Communications, vol. 326, pp. 80-87, Sept. 2014.

[9] H. Lee and J. Lee, "Joint clock and frequency synchronization for OFDM-based cellular systems," IEEE Signal Processing Letters, vol. 18, no. 12, pp. 757-760, Dec. 2011.

[10] M.F. Rabbi and C.C. Ko, "Timing jitter tracking for orthogonal frequency division multiple access system in high doppler spread," IET Communications, vol. 6, no. 11, pp. 1438-1446, Jul. 2012.

[11] B. Yang, K.B. Letaief, R.S. Cheng, and Z. Cao, "An improved combined symbol and sampling clock synchronization method for OFDM systems," IEEE Wireless Communications and Networking Conference, vol. 3, pp. 1153-1157, Sept. 1999.

[12] B. Ai, Z. Yang, C. Pan, J. Ge, Y. Wang, and Z. Lu, "On the synchronization techniques for wireless OFDM systems," IEEE Transactions on Broadcasting, vol. 52, no. 2, pp. 236-244, Jun. 2006.

[13] R.P. Giddings and J. M. Tang, "Experimental demonstration and optimisation of a synchronous clock recovery technique for real-time end-to-end optical OFDM transmission at 11.25Gb/s over 25km SSMF," Optics Express, vol. 19, no. 3, 2831-2845, Jan. 2011.

[14] M. Zhu, N. Cvijetic, M.F. Huang, T. Wang, and G.K. Chang, "Low-latency synchronous clock distribution and recovery for DWDM-OFDMA-based optical mobile backhaul," Journal of Lightwave Technology, vol. 32, no. 10, pp. 2012–2018, May 2014.

[15] Y. Cai, Q. Zhang, R. Chen, C. Kuang, Z. Zhang, Y. Li, and J. Chen, "An effective sampling clock synchronization method for continuous- and burst-mode transmission in OFDMA-PONs," Optics Communications, vol. 384, pp. 78-84, Feb. 2017.

[16] Z. Zhang, Q. Zhang, Y. Li, Y. Song, J. Zhang, and J. Chen, "A single pilot subcarrier-based sampling frequency offset estimation and compensation algorithm for optical IMDD OFDM systems," IEEE Photonics Journal, vol. 8, no. 5, pp. 1-9, Oct. 2016.

[17] Z. Zhang, Q. Zhang, J. Chen, Y. Li, and Y. Song, "Low-complexity joint symbol synchronization and sampling frequency offset estimation scheme for optical IMDD OFDM systems," Optics Express, vol. 24, no. 12, pp. 12577-12587, Jun. 2016.

[18] M. Chen, J. He, J. Tang, and L. Chen, "Pilot-aided sampling frequency offset estimation and compensation using DSP technique in DD-OOFDM systems," Optical Fiber Technology, vol. 20, no. 3, pp. 268-273, Jun. 2014.

[19] R. Deng, J. He, M. Chen, and L. Chen, "SFO compensation by pilot-aided channel estimation for real-time DDO-OFDM system," Optics Communications, vol. 355, pp. 172-176, Nov. 2015.

[20] H. Shafiee, B. Nourani, and M. Khoshgard, "Estimation and compensation of frequency offset in DAC/ADC clocks in OFDM systems," IEEE International Conference on Communications, vol. 4, pp. 2397-2401, Jun. 2004.

[21] R. Deng, J. He, M. Chen, Y. Wei, J. Shi, and L. Chen, "Real-time VLLC-OFDM HD-SDI video transmission system with TS-based SFO estimation," Optical Fiber Communications Conference and Exhibition, pp.1-3, Mar. 2017.

[22] T. Pollet, P. Spruyt, and M. Moeneclaey, "The BER performance of OFDM systems using non-synchronized sampling," IEEE Global Telecommunications Conference, vol. 1, pp. 253-257, Nov. 1994.

[23] B. Ai, Y. Shen, Z.D. Zhong, and B.H. Zhang, "Enhanced sampling clock offset correction based on time domain estimation scheme," IEEE Transactions on Consumer Electronics, vol. 57, no. 2, pp. 696-704, May 2011.

[24] F.M. Gardner, "Interpolation in digital modems. I. Fundamentals," IEEE Transactions on Communications, vol. 41, no. 3, pp. 501-507, Mar. 1993.

[25] L. Erup, F.M. Gardner, and R.A. Harris, "Interpolation in digital modems. II. Implementation and performance," IEEE Transactions on Communications, vol. 41, no. 6, pp. 998-1008, Jun. 1993.

[26] F. Harris, "Performance and design of Farrow filter used for arbitrary resampling," Proceedings of 13th International Conference on Digital Signal Processing, vol. 2, pp. 595-599, Jul. 1997.

[27] I. Neokosmidis, T. Kamalakis, J.W. Walewski, B. Inan, and T. Sphicopoulos, "Impact of nonlinear LED transfer function on discrete multitone modulation: analytical approach," Journal of Lightwave Technology, vol. 27, no. 22, pp. 4970-4978, Nov. 2009.

[28] A.M. Cailean, B. Cagneau, L. Chassagne, V. Popa, and M. Dimian, "Evaluation of the noise effects on visible light communications using Manchester and Miller coding," International Conference on Development and Application Systems, pp. 85-89, May 2014.